

This manuscript has been accepted for publication in *Measurement* following peer review. Please cite the published article as:

Zheng, X., Shi, B., Zhang, C.-C., Sun, Y., Zhang, L., & Han, H. (2021). Strain transfer mechanism in surface-bonded distributed fiber-optic sensors subjected to linear strain gradients: Theoretical modeling and experimental validation. *Measurement*, 179, 109510. <https://doi.org/10.1016/j.measurement.2021.109510>

Authors welcome comments, feedback, and discussions anytime. Please, feel free to contact the corresponding authors at shibin@nju.edu.cn (B.S.) or zhang@nju.edu.cn (C.-C.Z.).

Strain transfer mechanism in surface-bonded distributed fiber-optic sensors subjected to linear strain gradients: Theoretical modeling and experimental validation

Xing Zheng^a, Bin Shi^{a,*}, Cheng-Cheng Zhang^{a,b,c,*}, Yijie Sun^d, Lei Zhang^{a,e}, and Heming Han^a

^a School of Earth Sciences and Engineering, Nanjing University, Nanjing, Jiangsu 210023, China

^b Yuxiu Postdoctoral Institute, Nanjing University, Nanjing, Jiangsu 210023, China

^c Nanjing University High-Tech Institute at Suzhou, Suzhou, Jiangsu 215123, China

^d College of Transportation Science and Engineering, Nanjing Tech University, Nanjing, Jiangsu 210009, China

^e State Key Laboratory of Hydrosience and Engineering, Tsinghua University, Beijing 100084, China

* Correspondence to: shibin@nju.edu.cn (B.S.), zhang@nju.edu.cn (C.-C.Z.)

Abstract: Strain transfer analysis is an important means of assessing the measurement accuracy of embedded or surface-bonded fiber-optic sensors; however, the effect of complex strain fields in substrates has not been well elucidated. Here, a theoretical model was proposed for the analysis of strain transfer mechanisms in surface-bonded distributed fiber-optic sensors due to linear strain gradients. Closed-form solutions were obtained for both single linear and bilinear strain distributions, which were validated through controlled laboratory testing. High-resolution strain profiles acquired with optical frequency-domain reflectometry allowed also the establishment of a simple approach for determining the strain transfer coefficient at the turning point of a bilinear-type strain. Moreover, parametric analyses were conducted to investigate the influences of geometric and mechanical properties of protective and adhesive layers on the strain transfer efficiency, shedding light on the design, installation, and measurement accuracy improvement of fiber-optic sensors after accounting for the effect of substrate strain patterns.

Keywords: distributed fiber-optic sensor, shear lag, surface-bonding, strain transfer, optical frequency-domain reflectometry, sensing cable modeling

1. Introduction

Distributed fiber-optic (FO) sensing is a versatile tool for condition monitoring of civil and geotechnical structures because it offers advantages such as distributed and long-distance measurement capability, high precision, anti-interference, and easy installation [1–12]. Common sensing optical fibers are thin and fragile; hence, they usually require multi-layered sheath packaging to form FO cables or sensors to survive harsh environments [13–16]. While their robustness is improved, strain profiles will be altered by the process of strain transfer from a monitored substrate to the fiber core, affecting the measurement accuracy of a distributed FO strain sensing system [17–18]. Therefore, it is essential to understand the host-to-core strain transfer mechanism toward retrieving actual strain distributions in the monitored substrate.

The strain transfer theory of FO sensors has attracted a great deal of attention among researchers and practitioners on account of its significant importance. So far, most research achievements on this aspect have been established based on the shear lag theory of composite materials introduced by Cox [19]. The early research began with embedded FO sensors in engineering materials [20]. For example, Nanni et al. determined the strain transfer coefficient between FO sensor and concrete structure and found that the transfer coefficient will be higher when the Young's modulus of the protective layer is close to that of the fiber core [21]. In 1998, Ansari and Yuan established a strain transfer model of an embedded fiber Bragg grating (FBG) sensor due to a uniform strain field using the shear lag theory, which provides an important reference case for later theoretical analyses and engineering practices [16]. Li et al.

improved the model in ref. [16] based on the assumption that the strain gradient at the midpoint of each layer of FO sensor was approximately equal; the derived result was closer to the actual situation [17]. On this basis, strain transfer mechanisms in FBG sensors under nonaxial uniform strains were studied [22]. By introducing Goodman's hypothesis, Wang et al. further considered the influence of host viscoelasticity and ambient temperature on the strain transfer coefficient, which enriches the research on the strain transfer mechanism of embedded FO sensors [23].

Different from that of embedded FO sensors, analyzing the strain transfer for surface-bonded FO sensors should take into extra consideration the impacts of geometric and physical properties of the adhesive layer [24]. Wan et al. introduced an axisymmetric model of surface-bonded FBG sensor to investigate the influence of adhesive layer width and bottom thickness on the strain transfer coefficient, and the reliability of the model was validated through experiments and finite element analysis [25]. Considering the possible gap between FO cable and adhesive layer, Her et al. proposed an elaborate analytical model for strain transfer analysis of surface-bonded FO sensors [26,27]. Xin et al. derived a strain transfer model in the polar coordinate system and discussed the strain transfer phenomenon observed in crack detection [28]. Billon et al. developed a strain transfer function for concrete crack monitoring and the function was validated by the high-performance distributed FO sensing technology—optical frequency-domain reflectometry (OFDR) [29]. By also employing OFDR, Zhang et al. systematically investigated the effects of mechanical parameters and bonding method of FO cable on the strain transfer efficiency from both theoretical and

experimental sights [30]. More recently, Falcatelli et al. developed a strain transfer model of multi-layered FO cable and obtained the distribution of strain transfer coefficient for a nonzero boundary condition; the theoretical analyses were more consistent with actual observations [31].

From the above literature review, it can be found that current strain transfer theories are primarily developed for FBG sensors, and most studies have adopted the assumption that strain distributions in the host material are uniform. However, in actual structural health monitoring (SHM) or geotechnical applications, substrate strains are often complex and nonuniform. To this aim, a theoretical model was established for strain transfer analysis of surface-bonded distributed FO sensors with multi-layered structures subjected to linear strain gradients. Analytical solutions were derived for both single- and multi-linear type strain distributions. The proposed model was validated by two laboratory experiments with high-resolution strain profiles recorded using an OFDR interrogator. This study may provide a theoretical basis for the analysis of strain transfer mechanisms in surface-bonded distributed FO sensors due to nonuniform strain gradients in substrates and guide the design, installation, and measurement accuracy improvement of distributed FO sensors.

2. Strain transfer mechanism in surface-bonded distributed FO sensor

2.1. Model formulation

A distributed FO sensing system usually employs a packaged single-mode optical fiber—FO cable—as the sensing element and transmission medium. Deformation or

temperature profiles of a structure can be monitored by either bonding the distributed FO sensor on the structure surface or directly embedding it into the structure.

Extending the research of Falcetelli et al. [31], a theoretical model for strain transfer analysis of a surface-bonded FO sensor with an n -layered structure subjected to a nonuniform strain in the host material was established (Fig. 1). The proposed model is based on the following assumptions:

(1) Both the core and cladding of the sensor are silica, which can be regarded collectively as a single layer named fiber core.

(2) The fiber core, adhesive layer, and protective layers are all linear elastic materials; bonding conditions among different layers are good with no relative slippage.

(3) Only the shear stress transfer process among various layers within the bonded sensor length is considered.

The analytical model is established in the polar coordinate system where x represents the position along the axis of the sensor, r the radial position, and α the angle between the boundary point of the adhesive layer and the horizontal direction (see Fig. 1(a)). Referring to Fig. 1(b), the mechanical equilibrium of a fiber core element can be expressed as:

$$(\sigma_c + d\sigma_c)\pi r_c^2 - \sigma_c\pi r_c^2 + \int_0^{2\pi} \tau(x, r_c)r_c d\theta \cdot dx = 0 \quad (1)$$

where r_c is the outer radius of the fiber core layer, σ_c denotes the normal stress on the cross section of the fiber core, and $\tau(x, r_c)$ represents the shear stress at the interface between the fiber core and the first protective layer.

Eq. (1) can be readily reduced to the following:

$$\tau(x, r_c) = -\frac{r_c}{2} \frac{d\sigma_c}{dx} \quad (2)$$

According to assumption (3), the force equilibrium of the first protective layer leads to:

$$\int_{\alpha}^{\pi-\alpha} \tau(x, r) r d\theta \cdot dx - \int_0^{2\pi} \tau(x, r_c) r_c d\theta \cdot dx = 0 \quad (3)$$

where $\tau(x, r)$ represents the shear stress at the interface between the first and second protective layers. By combining Eqs. (2) and (3), $\tau(x, r)$ one gets:

$$\tau(x, r) = -\frac{\pi}{\pi - 2\alpha} \frac{r_c^2}{r} \frac{d\sigma_c}{dx} \quad (4)$$

Because the fiber core and each protective layer are assumed to behave linearly elastically during the strain transfer process (assumption (2)), the shear strain $\gamma(x, r)$ at the interface between the first and second protective layers, according to the Hooke's law, can be expressed as:

$$\gamma(x, r) = -\frac{1}{G_1} \frac{\pi}{\pi - 2\alpha} \frac{r_c^2}{r} E_c \frac{d\varepsilon_c}{dx} \quad (5)$$

where G_1 represents the shear modulus of the first protective layer, E_c is the Young's modulus of the fiber core, and ε_c denotes the normal strain of the fiber core. Since the radial displacement is far less than the axial displacement u , Eq. (5) can be alternatively written as:

$$\gamma(x, r) \cong \frac{\partial u}{\partial r} = -\frac{1}{G_1} \frac{\pi}{\pi - 2\alpha} \frac{r_c^2}{r} E_c \frac{d\varepsilon_c}{dx} \quad (6)$$

Then, the axial displacement on the boundary of the first protective layer can be obtained, by integrating Eq. (6) from r_c to r_1 , as follows:

$$\int_{r_c}^{r_1} \frac{\partial u}{\partial r} = \int_{r_c}^{r_1} -\frac{1}{G_1} \frac{\pi}{\pi-2\alpha} \frac{r_c^2}{r} E_c \frac{d\varepsilon_c}{dx} dr \quad (7)$$

$$u_1 - u_c = -\frac{1}{G_1} \frac{\pi}{\pi-2\alpha} r_c^2 E_c \frac{d\varepsilon_c}{dx} \ln \frac{r_1}{r_c} \quad (8)$$

where u_1 and u_c represent the axial displacement at the outer boundary of the fiber core and the first protective layer, respectively.

The same derivation is made for the other protective layers and the adhesive layer, and the following equation can be obtained:

$$u_h - u_c = -\frac{\pi}{\pi-2\alpha} r_c^2 E_c \frac{d\varepsilon_c}{dx} \left[\frac{1}{G_a} \ln \frac{r_a}{r_n} + \frac{1}{G_n} \ln \frac{r_n}{r_{n-1}} + \dots + \frac{1}{G_2} \ln \frac{r_2}{r_1} + \frac{1}{G_1} \ln \frac{r_1}{r_c} \right] \quad (9)$$

where u_h represents the axial displacement on the interface between the adhesive layer and the host; r_n and G_n represent the radius and shear modulus of the n th protective layer, respectively; G_a is the shear modulus of the adhesive layer; and r_a is the equivalent radius of the adhesive layer, which can be calculated according to the geometric characteristics of the model (Fig. 1(a)):

$$r_a = \frac{1}{\pi-2\alpha} \int_{\alpha}^{\pi-\alpha} [r_n (1 - \sin \alpha) + t] d\theta = r_n + t - \frac{2r_n \cos \alpha}{\pi-2\alpha} \quad (10)$$

where t represents the thickness of the adhesive layer from the sensor bottom to the host surface (see Fig. 1(a)). Here, a shear lag coefficient k is introduced, and then Eq.

(9) can be simplified as:

$$u_h - u_c = -\frac{1}{k^2} \frac{d\varepsilon_c}{dx} \quad (11)$$

where the coefficient k has the following form:

$$k = \sqrt{\frac{\pi-2\alpha}{\pi r_c^2 E_c \left[\frac{1}{G_a} \ln \frac{r_a}{r_n} + \frac{1}{G_n} \ln \frac{r_n}{r_{n-1}} + \dots + \frac{1}{G_2} \ln \frac{r_2}{r_1} + \frac{1}{G_1} \ln \frac{r_1}{r_c} \right]}} \quad (12)$$

Since the first derivative of axial displacement with respect to x is the axial

strain, Eq. (11) can be converted to:

$$\frac{d^2 \varepsilon_c}{dx^2} - k^2 \varepsilon_c = -k^2 \varepsilon_h(x) \quad (13)$$

where $\varepsilon_h(x)$ represents the strain distribution in the host material. The solution of Eq. (13) is obtained by solving the second order linear nonhomogeneous differential equation with constant coefficients:

$$\varepsilon_c(x) = C_1 e^{-kx} + C_2 e^{kx} + \varepsilon_h(x) \quad (14)$$

where C_1 and C_2 represent the integration constants that can be determined according to appropriate boundary conditions.

Finally, the strain transfer coefficient of the surface-bonded FO sensor can be defined as the ratio of the fiber core strain to the host strain, which is given by:

$$z(x) = \frac{\varepsilon_c}{\varepsilon_h} \quad (15)$$

2.2. Analytical solutions

2.2.1. Single linear gradient strain

When a cantilever beam with a uniform cross section is subjected to a point load at the free end, the strain distribution of the beam will be a single linear gradient.

Consider such a strain distribution as shown in Fig. 2, the corresponding strain transfer coefficient, with the boundary conditions $z(\pm L) = 0$, can be derived as:

$$z(x) = 1 - \frac{1}{ax + b} \left[\frac{aL \sinh(kx)}{\sinh(kL)} + \frac{b \cosh(kx)}{\cosh(kL)} \right] \quad (16)$$

where a and b represent the gradient and intercept of the imposed strain profile, respectively.

The influences of the bonding length $2L$ and the strain gradient a on the strain transfer coefficient of the FO sensor were studied through a simple example. In this example, three imposed strain distributions in the substrate were considered: $\varepsilon(x) = 5000$, $\varepsilon(x) = 2500x + 5000$, and $\varepsilon(x) = 5000x + 5000$, with a constant shear lag coefficient k of 6 m^{-1} . Similar to the case of a uniform host strain, the strain transfer coefficient profiles due to a single linear gradient strain are characterized by apparent low strain sensing sections—sensor segments with strain transfer coefficients being lower than 0.95—at both ends of the FO sensor (Fig. 3). When the bonding length of the FO sensor is larger than two times the length of the low strain sensing section (denoted as $2L_{\text{low}}$), the strain transfer performance in its middle portions will be good. Therefore, in practical applications, the bonded sensor length should be longer than $2L_{\text{low}}$ to avoid poor data quality. By contrast, when the shear lag coefficient k is small (corresponding to a poor strain transfer performance), the strain transfer profile will be directly affected by the strain distribution in the host material. Notably, the curves will incline to the side with a lower host strain, exacerbated by steeper gradients (see Fig. 3). These results collectively indicate that when the shear lag coefficient k is small at a given sensor design and installation scheme, the influence of host strain pattern on the strain transfer coefficient should be fully considered to retrieve actual strain profiles with higher accuracy.

2.2.2. Bilinear gradient strain

When a uniform beam is subjected to a three-point loading, its strain distribution will

be a combination of two linear strain gradients as shown in Fig. 4. In this case, the analytical solution of the strain transfer coefficient can only be derived if the coefficient value at the turning point of the bilinear curve (e.g., $x = 0$ in Fig. 4) is predetermined, in addition to the boundary conditions at the two sensor ends ($x = -L_1$, $x = L_2$). Assuming a transfer coefficient of z_0 at the turning point, the analytical solution is derived as:

$$z(x) = \begin{cases} 1 + \frac{(z_0 - 1) \cdot b \cdot \sinh[k(L_1 + x)] - (cL_1 - b) \sinh(kx)}{(ax + b) \cdot \sinh(kL_1)} & -L_1 \leq x \leq 0 \\ 1 + \frac{(z_0 - 1) \cdot b \cdot \sinh[k(L_2 - x)] - (aL_2 + b) \sinh(kx)}{(ax + b) \cdot \sinh(kL_2)} & 0 < x \leq L_2 \end{cases} \quad (17)$$

Considering the continuity of fiber strain along the axial direction, if both sensor sections (L_1-0 , $0-L_2$) are long enough ($> L_{low}$), it is reasonable to assume that the strain transfer coefficient at the turning point is 1. When the turning point falls within the low strain sensing section, however, it is difficult to obtain the strain transfer coefficient at the turning point.

In a numerical example we assumed that the host strain distribution was as follows:

$$\varepsilon(x) = \begin{cases} 1000x + 1000 & -L_1 \leq x < 0 \\ -1000x + 1000 & 0 \leq x \leq L_2 \end{cases} \quad (18)$$

Besides, we assumed that the strain transfer coefficient at the turning point was 0.95 to look at the strain transfer coefficient distribution (Fig. 5). It can be seen that the strain transfer profiles for single linear and bilinear gradient strains were of the same pattern. However, in actual applications, strain transfer coefficients at turning points remain unknown. Here, a simple method was proposed to solve this problem, which

can be described as following. First, the host strain distribution along the entire sensor length is assumed to have a gradient equivalent to the longer sensor section (e.g., the section $0-L_2$ in Fig. 4). Next, a hypothetical strain transfer distribution is obtained according to the method described in section 2.2.1. Then, the strain transfer coefficient at the turning point is extracted and taken as the definite solution for Eq. (17). Finally, the theoretical strain transfer coefficients along the whole bonding length are obtained. The feasibility of this approach will be verified by the laboratory tests described in the following section.

3. Experimental Validation

To validate the proposed analytical model, two laboratory tests were conducted where the host materials were subjected to multi-linear strains. In the first test, the sensor bonding length was made sufficiently long (each sensor section was longer than L_{low}) to examine whether the transfer coefficient can be set to 1 at the turning point in the theoretical model. The second test was aimed at exploring the determination of the turning point strain transfer coefficient in cases that the turning points are in the low strain section.

3.1. Three-point bending test of aluminum alloy inclinometer tube

3.1.1. Test setup and procedure

A three-point bending test was conducted on a 4 m long aluminum alloy inclinometer tube installed with a 0.9 mm diameter tight-buffered FO strain sensing cable (Fig. 6);

the test setup is shown in [Fig. 7](#). Table 1 summarizes the materials and parameters of the cable's components.

The FO cable was surface-adhered along the axial direction of the tube with epoxy resin. After the glue was cured, the inclinometer tube was symmetrically placed on two supports, and five dial gauges were installed at different positions above the pipe to record lateral displacements of the tube. The strain distributions of the cable were collected by an OSI-S OFDR interrogator with a spatial resolution of 1 mm and measurement accuracy of $\pm 1 \mu\epsilon$. More details about the principle of OFDR can be found in these works [\[36–39\]](#). The loading point was 2 m away from the left support and a 50 mm wide nylon belt was used for loading. The first loading applied was 16 kg with an increment of 25 kg, up to 141 kg in the sixth stage. After each loading stage was stable, the dial gauge and OFDR readings were respectively recorded to obtain the vertical displacement of the pipe and the strain profile of the cable.

3.1.2. Results and analysis

[Fig. 8](#) shows the lateral displacements of the inclinometer tube recorded by the dial gauges under each load. According to the theory of elasticity, the theoretical strain distributions of the tube were calculated from the lateral displacement measurements. On the other hand, the distributions of strain transfer coefficient were calculated using [Eq. \(16\)](#) by assuming perfect strain transfers at the turning point and were then used to correct the OFDR-measured strains. The calculated values of L_{low} were no more than 0.11 m, far less than the distances between each support and the loading point (2

m and 1.82 m, respectively). The parameters of the FO cable and adhesive layer used in the strain transfer analysis are listed in Table 1. These two strain profiles were compared (Fig. 9). The results show that except for the first loading stage, the corrected FO strains agreed well with the theoretical strains. It is noted that each strain curve had a ~50 mm wide flat section at its center, owing to the nylon belt used for loading. Despite this, there were no obvious low strain sensing sections at the turning point. Combined, this test validated the proposed model and the derived analytical solutions. Importantly, these observations supported the assumption that the strain transfer coefficient at the turning point can be set to 1 provided that the bonded FO cable is long enough (greater than $2L_{low}$) and the turning point of the host strain is not in any low sensing sections. Moreover, these results highlight the advantage of distributed FO sensing in large-scale SHM and geotechnical monitoring campaigns.

3.2. Three-point bending test of PVC pipe

3.2.1. Test setup and procedure

To further verify the established theoretical model and to seek a method for the determination of the transfer coefficient at the turning point in a low strain sensing section, an elaborate three-point bending test on a PVC pipe was carried out. A 3 m long PVC pipe with an outer diameter of 75 mm was used in the test. A G.652 double coating optical fiber manufactured by Corning Inc. was bonded on the surface of the pipe. The cable differs from the 0.9 mm tight-buffered cable in that there is no additional Hytrel jacket outside the coating. The OFDR interrogator used for FO

strain acquisition was a Luna OBR 4413. The spatial resolution was 10 mm and the strain measurement accuracy was $\pm 5 \mu\epsilon$.

The test setup is shown in [Fig. 10](#). Two FO cables AB (orange) and ab (red) were bonded in parallel on the lower surface of the PVC pipe with epoxy resin. A redundant section was reserved at 0.1 m to the left of the loading point. The two ends of the PVC pipe were fixed by hinge supports. The pipe was deformed by hanging heavy objects in its middle part. The load from the first stage to the fourth stage was increased by 3 kg per stage, while the fifth stage and sixth stage were increased by 6 kg per stage.

3.2.2. Results and analysis

Strain distributions of the two FO cables obtained by the OFDR interrogator are shown in [Fig. 11](#). The strain curves of cable AB exhibited symmetrical triangle distributions, and the position of the maximum strain point was consistent with the loading point. The strain curves of cable ab were divided into three sections—bc section, redundant section, and ac section.

Comparisons of strain values between sections BC and bc and those between sections AC and ac are shown collectively in [Fig. 12](#). Although most strains of the two cables were consistent, the deviations observed in the vicinity of point c were indicative of the existence of low strain sensing sections at the free end. According to the conclusions drawn in section 3.1 and considering that cable AB was sufficiently long, its strain values may be regarded as the true strains of the pipe. Therefore, the experimental strain transfer coefficients of section bc (or ac) can be determined by

comparing its strain values to those of section BC (respectively, AC).

For the theoretical strain transfer coefficients of section bc, because the strain distributions of the pipe were of the single linear gradient strain type (as indicated by the strain measurements of cable BC), they can be readily calculated using Eq. (16). A comparison between the experimental and theoretical strain transfer coefficients under the sixth loading stage (24 kg) is shown in Fig. 13. The parameters of the FO cable and adhesive layer used in the theoretical analysis were the same as those listed in Table 1 (except for the jacket). It can be seen from Fig. 13 that the two coefficient curves coincided with each other, hence validating the proposed theoretical model.

For the theoretical strain transfer coefficients of section ac, because the strain distributions of the pipe were of the bilinear gradient strain type (as indicated by the strain measurements of cable AC), determining the strain transfer coefficient at the turning point (i.e., loading point) was a prerequisite. In this test, the length of the low strain sensing section (L_{low}) of the cable was about 0.11 m according to the experimental results of cable bc, which was longer than the distance between the loading point and point c (0.1 m). Hence, the method proposed in section 2.2.2 was employed to determine the theoretical strain transfer coefficient distribution. The calculated z_0 is 0.954 and a comparison between the calculated and experimental strain transfer coefficient profiles of cable ac under the sixth loading is shown in Fig. 14. Good agreement between the two curves illustrated the feasibility of the proposed method for evaluating the strain transfer performance of surface-bonded distributed FO sensors subjected to bilinear gradient strains in substrates.

4. Parametric study

To provide practical suggestions on the design and installation of distributed FO strain sensors, the influences of mechanical and geometric parameters of protective and adhesive layers on the strain transfer efficiency were analyzed according to Eq. (16).

The distribution of host strain was assumed to be a single linear gradient strain $\varepsilon(x) = 1000x + 1000$, and the bonding length of the sensor was 1 m. The parameters of the sensor and adhesive layer used in this parametric study were consistent with those used in section 3.2.2.

The influence of the shear modulus of the inner coating G_1 on the strain transfer coefficient is shown in Fig. 15. With the increase of G_1 , the length of the low strain sensing section at both ends decreased, and the strain transfer performance of the sensor was greatly improved. Therefore, when designing strain sensing sensors, the coating materials with higher shear modulus should be selected to reduce the adverse effect of coating on the strain measurement performance of the sensor. Similarly, the effect of the shear modulus of the outer coating G_2 was investigated. For $G_2 = 50, 600,$ and 1200 MPa, the calculated values of the shear lag coefficient k were 31.79, 31.81, and 31.81 m^{-1} , respectively. The higher the shear modulus of the outer coating, the higher the value of k and the better the strain transfer performance were. However, its influence was far less evident compared to that of the inner coating. Specifically, the results of $G_2 = 600$ and 1200 MPa were almost the same, indicating that the protective layer and especially the outer coating can protect the glass core with a limited impact

on its strain transfer performance.

The effects of the shear modulus G_a and minimum thickness t of the adhesive layer were also examined. For $G_a = 2.9, 29, \text{ and } 290$ MPa, the calculated shear lag coefficients k were 30.88, 31.79, and 31.88 m^{-1} , respectively. Therefore, the strain transfer performance of the FO sensor will be slightly better for a stiffer adhesive layer. The minimum thickness t was set to 20, 200, and 2000 μm ; the calculated shear lag coefficients were 32.00, 31.79, and 31.47 m^{-1} , respectively. The results indicate that a thicker adhesive layer will reduce the strain transfer performance of the sensor but the impact is also limited. Considering that the adhesive can “protect” the surface-bonded FO sensor, the thickness of the adhesive layer can be increased appropriately without significantly decreasing the sensor’s sensing performance. Similarly, in the process of designing and producing strain sensing cables, high shear modulus protective layers can be adopted and their thicknesses can be increased properly to improve the sensor’s robustness while ensuring its strain transfer performance. However, we note also that because a stiff sheath will reduce the sensor’s ability to measure maximum peak strains, the shear modulus of the sheath should be controlled within a reasonable value.

5. Conclusions

In this paper, the strain transfer mechanism between a surface-bonded multi-layered distributed FO sensor and a substrate structure was examined with the consideration of nonuniform strain fields in the substrate. A theoretical model was established for

the analysis of host-to-fiber strain transfer due to single linear and bilinear strain gradients. In particular, a simple approach was proposed for the determination of strain transfer coefficients at the turning points of a multi-linear strain distribution. Two laboratory tests were conducted to validate the proposed method. Once the developed model was verified, a parametric study was performed to investigate the influences of host strain distribution and mechanical and geometric characteristics of protective and adhesive layers on the sensor's strain transfer performance. The main findings of this study are the following:

- The influence of host strain distribution on the host-to-fiber strain transfer efficiency is mostly restricted to the low strain sensing sections (with length denoted by L_{low}) at both ends of the bonded sensor. When the bonding length is short or the shear lag coefficient is low (large L_{low}), the effect of host strain patterns should be considered in evaluating the strain transfer quality.
- For a single linear strain gradient in the substrate, the value of L_{low} at the lower strain end decreases (while that at the other end increases) with an increasing gradient.
- In cases of multi-linear strain gradients in the host material, when each sensor section is longer than L_{low} the strain transfer coefficients of the turning points can be set to 1. For turning points falling within a low strain sensing section, their transfer coefficients can be approximated by analyzing a hypothetical host strain distribution having a gradient equivalent to that of the longer sensor section.
- The parametric analyses show that the strain transfer performance of the FO

sensor can be improved by employing coating materials of high shear moduli, but the effect of protective layers on the strain transfer efficiency is relatively insignificant. Therefore, while ensuring the sensor's ability to measuring maximum peak strains, the shear moduli and radii of protective layers can be appropriately improved to allow the sensor to survive harsh environments. Moreover, to improve the measurement accuracy, stiff adhesives are recommended, the bonding length should be longer than $2L_{low}$, and the sensor should be adhered close to the substrate surface.

Acknowledgments

We thank Xing Wang and the staff of Suzhou NanZee Sensing Technology Ltd. for their technical assistance. We acknowledge constructive reviews by seven anonymous reviewers which led to substantial improvement of the manuscript. This work was supported by the National Natural Science Foundation of China (NSFC) grant 42030701 (to B.S.) and the Natural Science Foundation of Jiangsu Province grant BK20200217 (to C.-C.Z.). C.-C.Z. acknowledges additional support from the National Key R&D Program of China grant 2019YFC1509601, the Fundamental Research Funds for the Central Universities grant 020614380110, and the Yuxiu Young Scholars Program of Nanjing University. Y.S. acknowledges support from NSFC grant 41702315. L.Z. acknowledges support from an open fund provided by the Hebei IoT Monitoring Engineering Technology Research Center grant IOT202005.

References

- [1] H.N. Li, D.S. Li, G.B. Song, Recent applications of fiber optic sensors to health monitoring in civil engineering. *Engineering Structures*, 2004, 26(11): 1647-1657.
- [2] X.Y. Bao, L. Chen, Recent progress in distributed fiber optic sensors. *Sensors*, 2012, 12(7): 8601-8639.
- [3] H.F. Pei, J. Teng, J.H Yin, R. Chen, A review of previous studies on the applications of optical fiber sensors in geotechnical health monitoring. *Measurement*, 2014. 58: 207-214.
- [4] A. Barrias, J. R. Casas, S. Villalba, A review of distributed optical fiber sensors for civil engineering applications. *Sensors*, 2016. 16(5): 748.
- [5] H. Mohamad, K. Soga, A. Pellew, P.J. Bennett, Performance monitoring of a secant-piled wall using distributed fiber optic strain sensing. *Journal of Geotechnical and Geoenvironmental Engineering*, 2011. 137(12): 1236-1243.
- [6] H. Mohamad, K. Soga, P.J. Bennett, R.J. Mair, S.L. Chi, Monitoring twin tunnel interaction using distributed optical fiber strain measurements. *Journal of Geotechnical and Geoenvironmental Engineering*, 2012, 138(8):957-967.
- [7] C.C. Zhang, H.H. Zhu, Q. Xu, B. Shi, G.X. Mei, Time-dependent pullout behavior of glass fiber reinforced polymer (GFRP) soil nail in sand. *Canadian Geotechnical Journal*, 2015, 52(6):671-681.
- [8] Z.P. Song, D. Zhang, B. Shi, S.E. Chen, M.F. Shen, Integrated distributed fiber optic sensing technology-based structural monitoring of the pound lock. *Structural Control and Health Monitoring*, 2017, 24(7), e1954
- [9] X. Wang, B. Shi, G.Q. Wei, S.E. Chen, H.H. Zhu, T. Wang, Monitoring the

behavior of segment joints in a shield tunnel using distributed fiber optic sensors.

Structural Control and Health Monitoring, 2018, 25(1): 2056.

[10] L. Pelecanos, K. Soga, M.Z.E.B. Elshafie, N.D. Battista, C. Kechavarzi, Y.G.

Chang, Y. Ouyang, H.J. Seo, Distributed fiber optic sensing of axially loaded bored piles. Journal of Geotechnical and Geoenvironmental Engineering, 2018,

144(3):04017122.1-04017122.16.

[11] H. Wu, H.H. Zhu, C.C. Zhang, G.Y. Zhou, M. Azarafza, Strain integration-based soil shear displacement measurement using high-resolution strain sensing technology.

Measurement, 2020, 166, 108210.

[12] P. Velha, T. Nannipieri, A. Signorini, et al., Monitoring large railways

infrastructures using hybrid optical fibers sensor systems. IEEE Transactions on

Intelligent Transportation Systems, 2020, 21(12):5177-5188

[13] C.Y. Hong, Y.F. Zhang, G.W. Li, M.X. Zhang, Z.X. Liu, Recent progress of using

Brillouin distributed fiber sensors for geotechnical health monitoring. Sensors &

Actuators A Physical 2017, 258:131-145.

[14] H.P. Wang, P. Xiang, L. Jiang, Strain transfer theory of industrialized optical

fiber-based sensors in civil engineering: A review on measurement accuracy, design

and calibration. Sensors and Actuators A: Physical, 2019, 285: 414-426.

[15] F. Bastianini, R. Di Sante, F. Falcatelli, D. Marini, G. Bolognini, Optical fiber

sensing cables for Brillouin-based distributed measurements. Sensors, 2019, 19(23):

5172.

[16] C.C. Zhang, B. Shi, H.H. Zhu, B.J. Wang, G.Q. Wei, Toward distributed fiber-

- optic sensing of subsurface deformation: A theoretical quantification of ground-borehole-cable interaction. *Journal of Geophysical Research: Solid Earth*, 2020, 125(3), e2019JB018878.
- [17] F. Ansari, L.B. Yuan, Mechanics of bond and interface shear transfer in optical fiber sensors. *Journal of Engineering Mechanics*, 1998, 124(4):385-394.
- [18] D.S. Li, Strain transferring analysis of fiber Bragg grating sensors. *Optical Engineering*, 2006, 45(2):409-411.
- [19] H.L. Cox, The elasticity and strength of paper and other fibrous materials[J]. *British Journal of Applied Physics*, 1951, 3(3):72.
- [20] G. Duck, M. Leblanc, Arbitrary strain transfer from a host to an embedded fiber-optic sensor. *Smart Materials and Structures*, 2000. 9(4): 492-497.
- [21] A. Nanni, C.C. Yang, K. Pan, J.S. Wang, R.R.M. Jr, Fiber-optic sensors for concrete strain/stress measurement. *ACI Materials Journal*, 1991, 88(3):257-264.
- [22] H.N. Li, Strain transfer analysis of embedded fiber Bragg grating sensor under nonaxial stress. *Optical Engineering*, 2007, 46(5): p. 054402-054408.
- [23] H.P. Wang, P. Xiang, Strain transfer analysis of optical fiber based sensors embedded in an asphalt pavement structure. *Measurement Science and Technology*, 2016, 27(7): 75106.
- [24] G. Duck, G. Renaud, R. Measures, The mechanical load transfer into a distributed optical fiber sensor due to a linear strain gradient: embedded and surface bonded cases. *Smart Materials and Structures*, 1999, 8(2): 175-181.
- [25] K.T. Wan, Quantitative sensitivity analysis of surface attached optical fiber strain

sensor. *IEEE Sensors Journal*, 2014, 14(6): 1805-1812.

[26] S.C. Her, C.Y. Tsai, Strain measurement of fiber optic sensor surface bonding on host material. *Transactions of Nonferrous Metals Society of China*, 2009, 19(z1): 143-149.

[27] S.C. Her, C.Y. Huang, Effect of coating on the strain transfer of optical fiber sensors. *Sensors*, 2011. 11(7): 6926-6941.

[28] F. Xin, Z. Jing, C. Sun, X. Zhang, F. Ansari, Theoretical and experimental investigations into crack detection with BOTDR-distributed fiber optic sensors. *Journal of Engineering Mechanics*, 2013, 139(12): 1797-1807.

[29] A. Billon, J.-M. Henault, M. Quiertant, F. Taillade, A. Khadour, R.-P. Martin, K. Benzarti², Quantitative strain measurement with distributed fiber optic systems: Qualification of a sensing cable bonded to the surface of a concrete structure. *EWSHM - 7th European Workshop on Structural Health Monitoring*, 2014, 1941-1948.

[30] Q. Zhang, Y. Sun, Z. Zhang, P. Zeng, F. Rong, Strain transfer in distributed fiber optic sensor with optical frequency domain reflectometry technology. *Optical Engineering*, 2019, 58(2).

[31] F. Falcetelli, L. Rossi, R. Di Sante, G. Bolognini, Strain transfer in surface-bonded optical fiber sensors. *Sensors (Basel)*, 2020, 20(11).

[32] Y. P. Michel, M. Lucci, M. Casalboni, P. Steglich and S. Schrader, Mechanical characterisation of the four most used coating materials for optical fibres.

International Conference on Photonics, Optics and Laser Technology

(PHOTOPTICS), Berlin, Germany, 2015: 91-95.

[33] S.H. Kim, J.J. Lee, I.B. Kwon, FEM analysis of surface-mounted distributed optical fiber sensors. 2001: SPIE.

[34] S.M. Wei, J. Chai, Surface pasting methods and analyses of strain transfer in rock deformation tests using FBG. Chinese Journal of Geotechnical Engineering, 2011.33(4):578-592. (in Chinese)

[35] Z. Zhang, Y. Wang, Y. Sun, Q. Zhang, Z. You, X. Huang, Analysis and experimental study on the strain transfer mechanism of an embedded basalt fiber-encapsulated fiber Bragg grating sensor. Optical Engineering, 2017. 56(1):017105.

[36] J.H. Wu, H. Liu, P. Yang, B.J. Tang, G.Q. Wei, Quantitative strain measurement and crack opening estimate in concrete structures based on OFDR technology. Optical Fiber Technology, 2020, 60:102354.

[37] M. Froggatt, J. Moore, High-spatial-resolution distributed strain measurement in optical fiber with rayleigh scatter. Applied Optics, 1998, 37(10):1735-40.

[38] S.T. Kreger, D.K. Gifford, M.E. Froggatt, B.J. Soller, M.S. Wolfe, High resolution

distributed strain or temperature measurement in single-mode fiber using swept-wavelength interferometry, 18th International Conference Optical Fiber Sensing, 2006.

[39] J.M Henault, G. Moreau, S. Blairon, J. Salin, J.R. Courivaud, F. Taillade, E. Merliot, J.P. Dubois, J. Bertrand, S. Buschaert, S. Mayer, S. Delepine-Lesoille, Truly distributed optical fiber sensors for structural health monitoring: From the

telecommunication optical fiber drawling tower to water leakage detection in dikes and concrete structure strain monitoring. *Advances in Civil Engineering*, 2010, 2010:13.

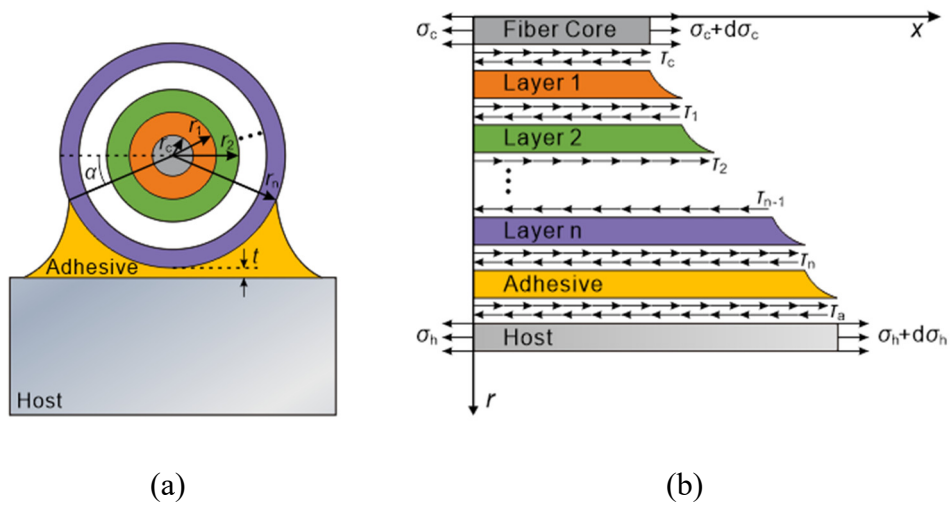


Fig. 1. Strain transfer mechanism in a surface-bonded multi-layered distributed FO sensor. (a) Cross section. (b) Stress state of a cable element.

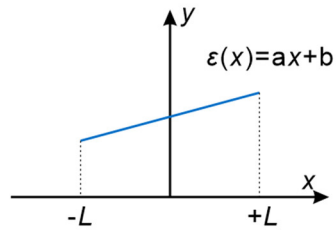


Fig. 2. Schematic diagram of a single linear gradient strain.

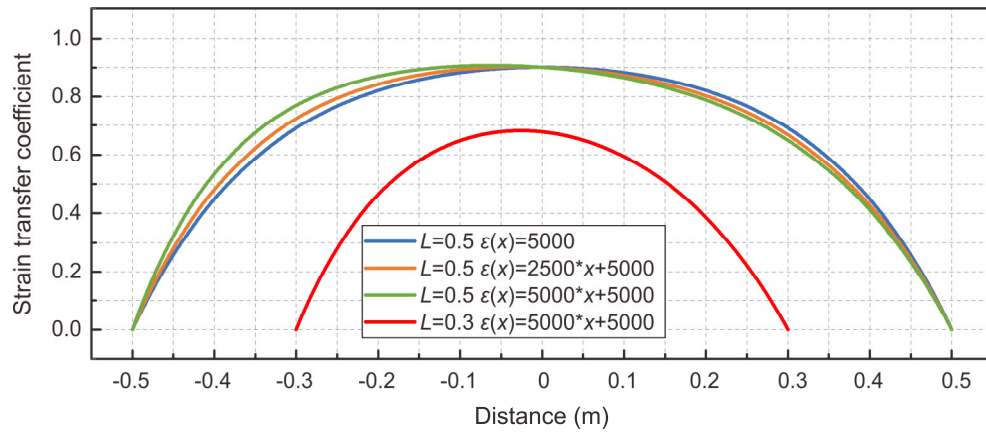


Fig. 3. Influence of bonding length and strain gradient on the strain transfer coefficient.

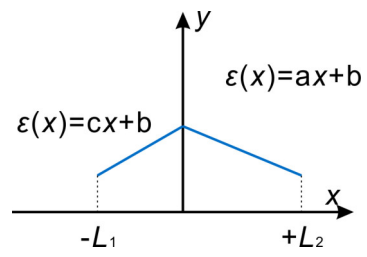


Fig. 4. Schematic diagram of a bilinear gradient strain.

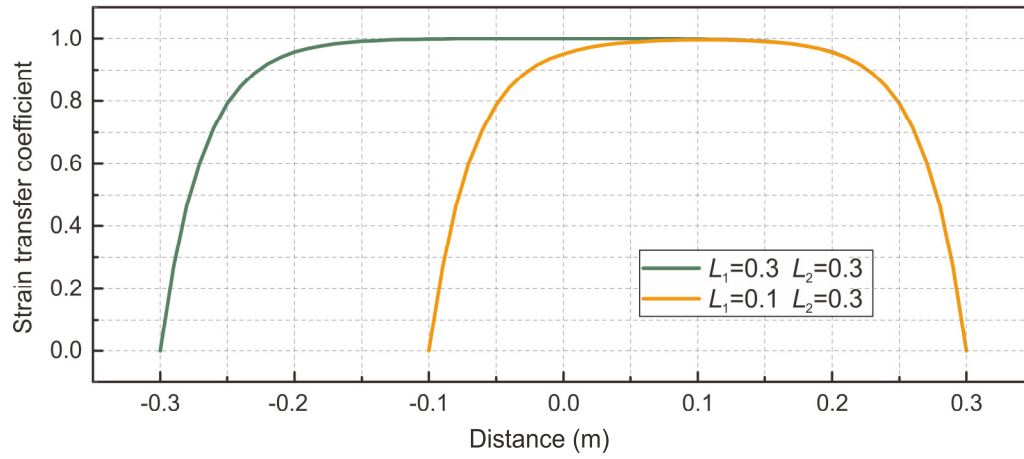


Fig. 5. Analytical distributions of strain transfer coefficient subjected to a bilinear host strain.

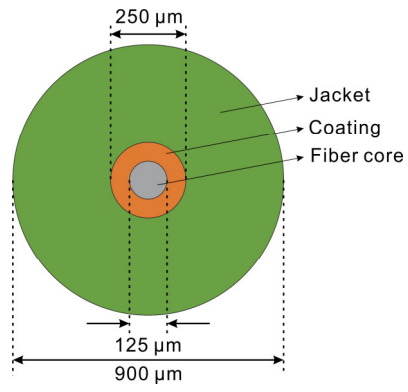


Fig. 6. Structure of a 0.9 mm diameter tight-buffered FO strain sensing cable.

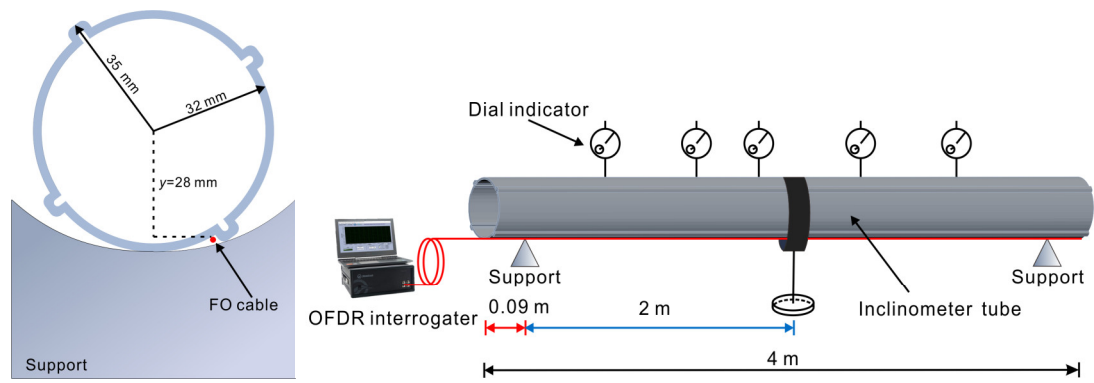


Fig. 7. Schematic of three-point bending test of inclinometer tube.

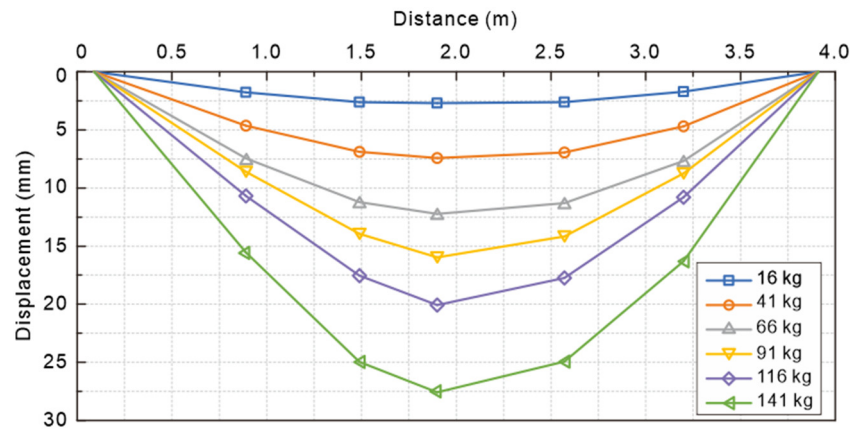


Fig. 8. Lateral displacements of inclinometer tube recorded by dial gauges.

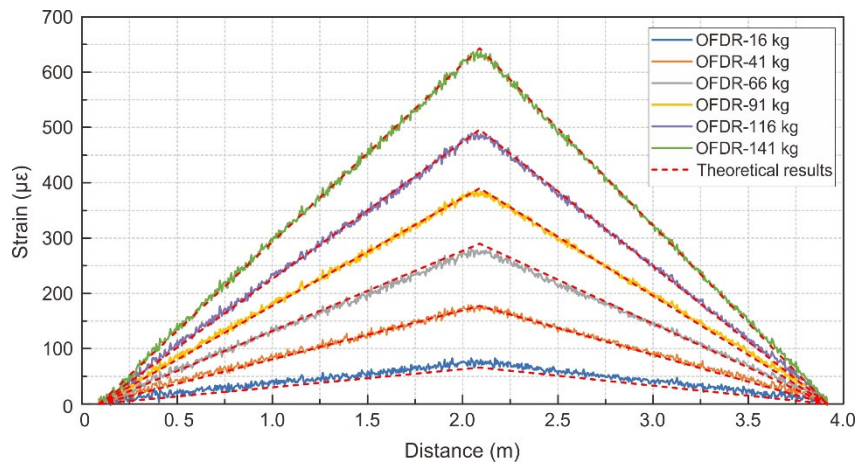


Fig. 9. Comparison of experimental (FO) and theoretical strain distributions along inclinometer tube. The FO strains were corrected according to calculated strain transfer coefficients.

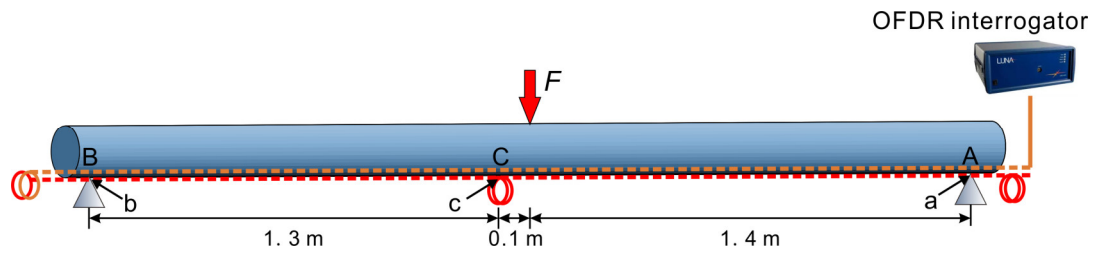


Fig. 10. Schematic of three-point bending test of PVC pipe.

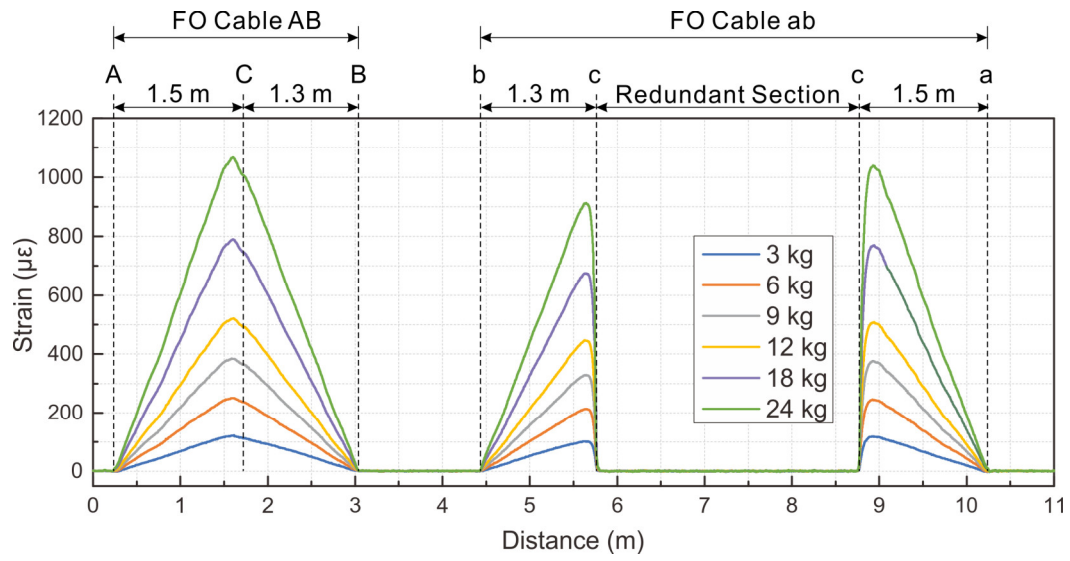


Fig. 11. Strain distributions acquired by FO cables under each load.

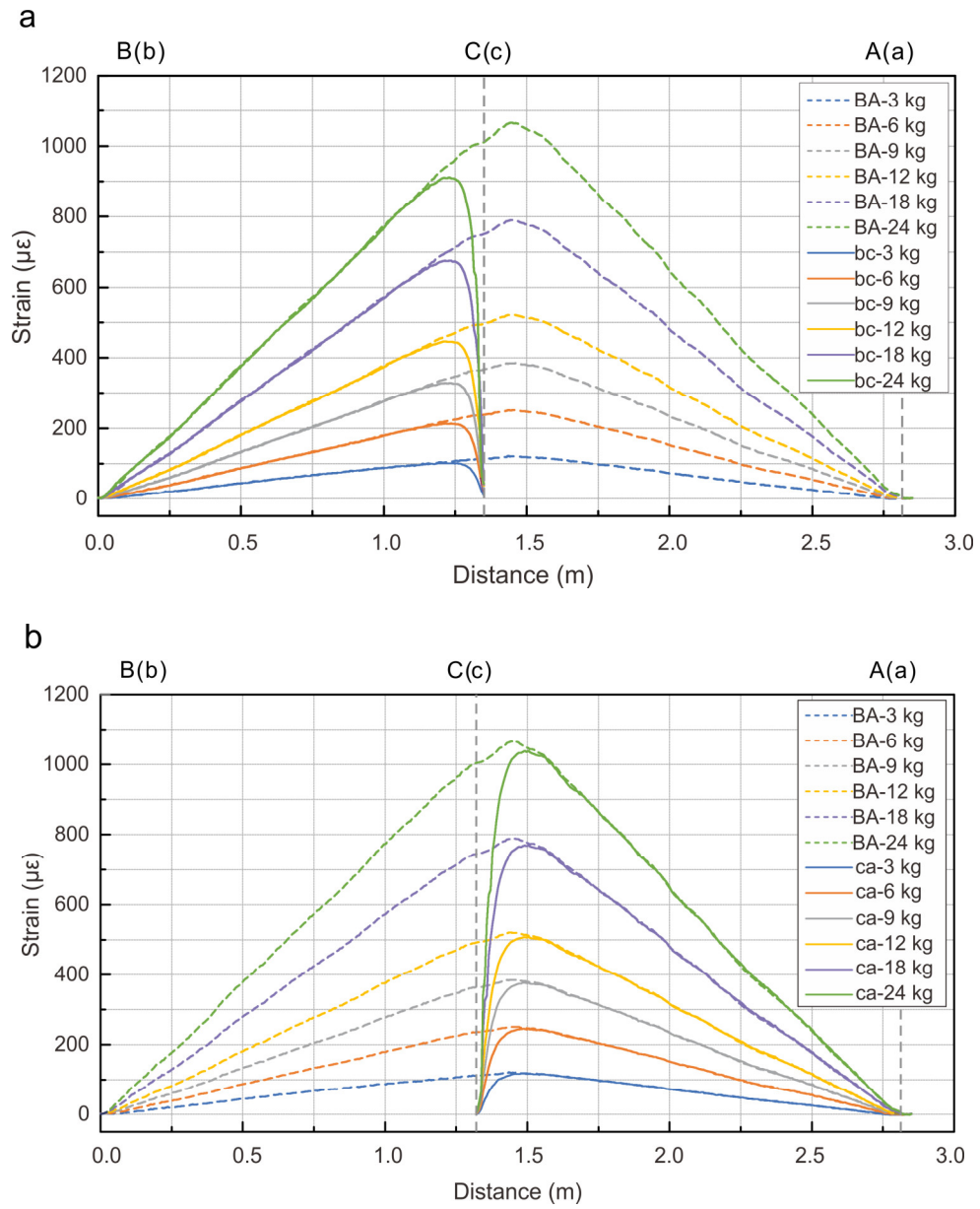


Fig. 12. Comparison of strain distributions between cables AB and ab.

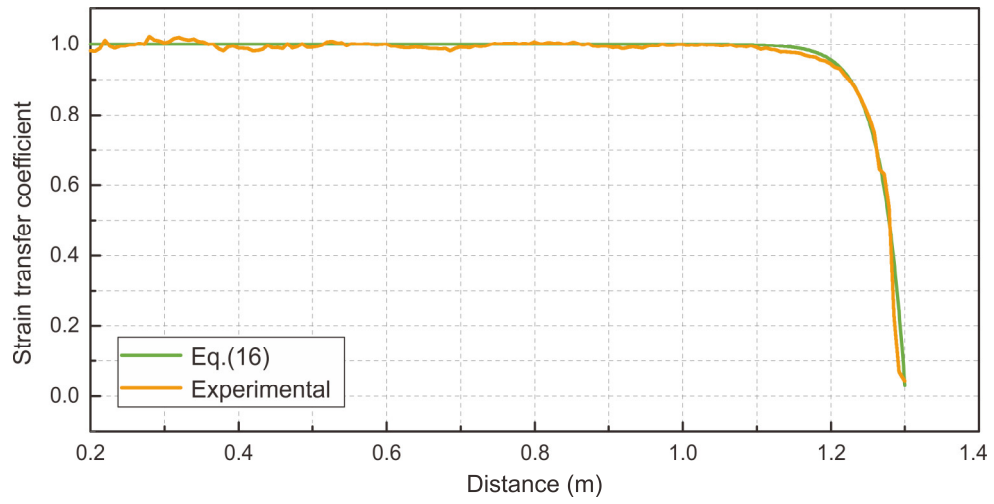


Fig. 13. Comparison between experimental and theoretical strain transfer coefficient distributions for cable bc.

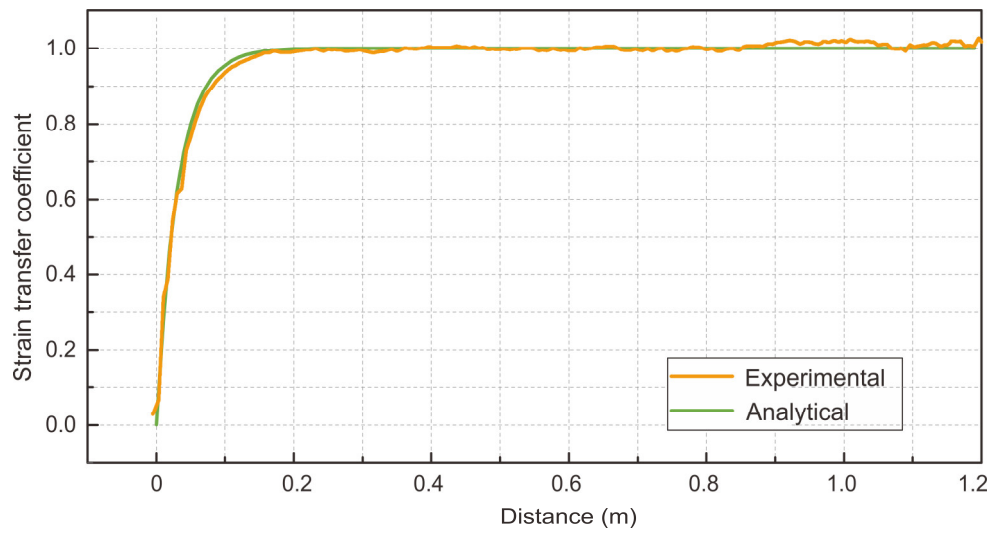


Fig. 14. Comparison between experimental and theoretical strain transfer coefficient distributions for cable ac.

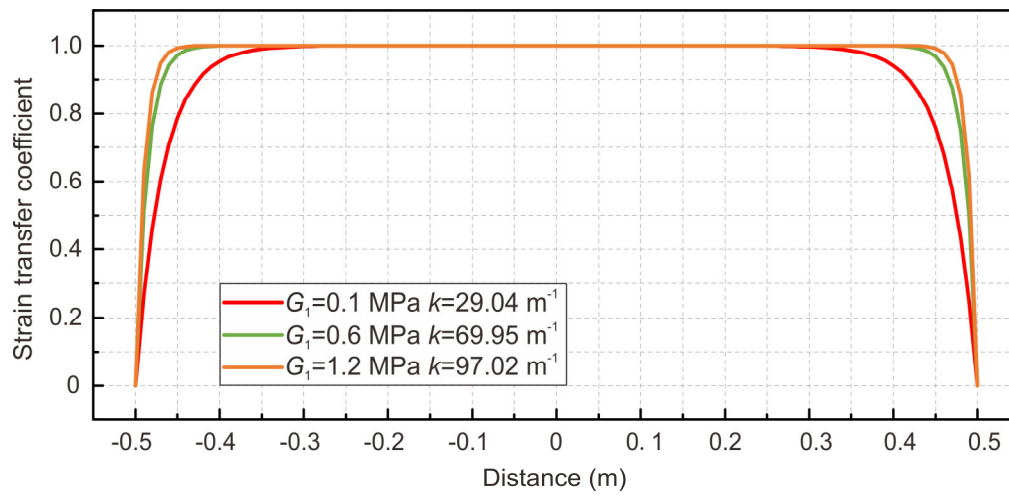


Fig. 15. Influence of shear modulus of inner coating on the strain transfer efficiency of FO sensor.

Table 1. Component materials and parameters of FO cable and adhesive layer used for strain transfer coefficient calculation (after refs. [17, 18, 32–35]).

Layer	Materials	Parameter	Symbol	Value	Unit
Fiber core	Silica	Radius	r_c	62.5	μm
		Young's modulus	E_c	72	GPa
Inner coating	Soft Acrylate	Radius	r_1	95	μm
		Shear modulus	G_1	0.12	MPa
Outer coating	Stiff Acrylate	Radius	r_2	125	μm
		Shear modulus	G_2	50	MPa
Jacket	Hytrel	Radius	r_3	900	μm
		Shear modulus	G_3	500	MPa
Adhesive	Epoxy resin	Minimum thickness	t	200	μm
		Shear modulus	G_a	29	MPa